IEEE Access
Multidisciplinary | Rapid Review | Open Access Journal

IEEE MAGNETICS SOCIETY SECTION

Received February 8, 2022, accepted March 1, 2022, date of publication March 23, 2022, date of current version March 31, 2022.

Digital Object Identifier 10.1109/ACCESS.2022.3161633

Dynamic Analysis of Surface-Mounted Permanent Magnet Type Coaxial Magnetic Gear With Damper Bar Considering Magnetic Field Modulation Effect

SEOKHOON JO[1], (Student Member, IEEE), HOMIN SHIN[2], (Member, IEEE), AND JUNGHWAN CHANG[1], (Member, IEEE)

[1]Mechatronics System Research Laboratory, Department of Electrical Engineering, Dong-A University, Busan 49315, South Korea
[2]Department of Electrical Engineering, Masan University, Changwon 51217, South Korea

Corresponding author: Junghwan Chang (cjhwan@dau.ac.kr)

This work was supported by the Railway Vehicle Parts Development Project of Korea Agency for Infrastructure Technology Advancement (KAIA) funded by the Ministry of Land, Infrastructure and Transport of Korean Government under Grant 21RSCD-C160566-01.

ABSTRACT Coaxial Magnetic Gear (CMG) has unstable dynamic characteristics by hunting or pull-out action of the output rotor when the load or speed are changed, unlike traditional mechanical gears. These dynamic characteristics need to be improved in order to secure the reliability of mechanical power transmission system by fast and accurate response. In this paper, the damper bar used in synchronous machines is considered as a method to improve the dynamic characteristics of CMG. The Surface-mounted Permanent Magnet (SPM) type CMG is selected as the analysis model. The space harmonics of the magnetic flux density of stationary and rotary members of CMG namely, modulating pieces, inner and outer rotor, are analyzed and characterized the influence of them on the improvement of dynamic characteristics as well as torque reduction. Also, the magnetic flux density characteristics and the damping effect are compared according to the position of the damper bars on two rotors and the modulating pieces. In conclusion, the considerations about the perspective for design and application are presented when using the damper bar for SPM type CMG.

INDEX TERMS Coaxial magnetic gear, damper bar, dynamic analysis, magnetic field modulation effect, space harmonics.

I. INTRODUCTION

In applications employing rotating devices, gear mechanism is frequently used to produce acceleration/deceleration, rotational direction conversion, and rotational axis conversion, etc. The commonly used mechanical gears transmit power through the physical contact of the teeth. For this reason, the use of mechanical gears creates losses in the form of friction, heat, vibration, and noise. Hence, the mechanical gears should undergo periodic maintenance and various efforts have been continuously executed to reduce mechanical losses in such gears [1]–[5]. Since decades ago, some researchers have proposed the concept of magnetic gear, which transmits power through the magnetic field and it can be used as a solution to overcome the drawbacks of mechanical gears [6], [7]. Although the magnetic gear can solve the disadvantages arised from physical contact, further research on selecting the efficient topology of the magnetic gear is needed due to their low torque density. Among these studies, in particular, the application of the Coaxial Magnetic Gear (CMG) topology, proposed by Atallah *et al.* in 2001 significantly improved torque density [8]. By applying the magnetic field modulation effect, the CMG can change the gear ratio and direction of rotation of input and output rotors. Furthermore, CMG has great advantages in fields such as wind power generation, marine, and aerospace propulsion systems that enhance performances by using counter rotating propellers [9]–[12]. For this reason, a number of researches have been performed with various designs and experimentations to improve the performance of CMG [13]–[23].

The associate editor coordinating the review of this manuscript and approving it for publication was Montserrat Rivas.

However, the advantages of non-contact operation of the magnetic gear including CMG can also act as a source of disadvantage in system reliability during dynamic motion. When the stiffness of the teeth of the mechanical gear is compared with the magnetic coupling force of a CMG to identify dynamic characteristics, following problems are present.

1) As the teeth of the mechanical gears has extremely high stiffness than magnetic coupling force of the magnetic gears, load fluctuations or speed changes do not affect the gear ratio of input and output sides. However, magnetic gears have a ''hunting' action in which the rotors of the input and output adjust the new load angle and speed ratio when a load change or speed change occurs. This is an obvious disadvantage of magnetic gears in applications that require fast response between input and output sides.
2) In the mechanical gear, if the teeth between the input and output gears are damaged by an overload it cannot transmit power to the output gear. However, once an overload occurs beyond the pull-out torque of the CMG, the input and output are completely out of synchronization and the state of the output gear is unpredictable. During this asynchronous operation, the movement of the output rotor is exposed to continuously pulsating force by non-periodic magnetic field. In addition, the modulating pieces (MPs), which are responsible for the airgap magnetic field modulation, produce vibration and noise due to rapid changes in magnetic forces.

The previously stated ''hunting'' and ''pull-out'' conditions also occur in synchronous machine including Permanent Magnet Synchronous Machine (PMSM). Occasionally, these machines are equipped with conductor bars called damper bars which act as squirrel-cage winding in induction machine [24]–[28]. These damper bars perform not only for line starting of synchronous machine but also for improving dynamic motion by damping of torque oscillations. This is because of the induced current produced by the rotating magnetic field by the stator winding current of the PMSM. When the rotor is not synchronized with the rotating magnetic field due to load and speed fluctuations, the magnetic field induces the current to the damper bars. The induced current creates a reaction magnetic field in the direction that prevents the hunting and pull-out of the rotor. When the rotor is synchronized with the rotating magnetic field again, only the harmonics induce current in the damper bars. However, due to the magnetic field modulation, there is an abundance of space harmonics in the airgap magnetic flux density of CMGs, and they have large amplitude. In particular, in the CMG with high gear ratio, the amplitudes of unmodulated space harmonics are bigger than that of working harmonic occasionally. The asynchronous harmonics including the unmodulated harmonics rotate at different speed with respect to the rotor even during the steady state and result in continuous damping torque, which degrades the performance of the CMG.

Until recently, various studies have been conducted to predict or improve the dynamic characteristics of CMG. The work in [29] investigated the dynamic behavior of CMG according to the operating conditions such as start-up, abrupt load change, and dynamic pull-out condition using an analytical model. The researches in [30], [31] performed the study to predict the dynamic behavior with a block diagram by modeling the motion equation of CMG. The works in [32]–[34] suggest the application of damper bars in CMG. However, state of the art research does not provide information on how the magnetic field modulation characteristic is effected by the use of damper bar in CMG. They only include topology comparison and parametric study to enhance the dynamic characteristics of the CMG with damper bar. In addition, although the CMG can have three rotary members namely, MPs, inner and outer rotor, these papers have presented studies of inserting damper bars into the inner rotor only without proper explanations. However, due to the magnetic field modulation, an abundance of space harmonics is generated in the airgap, Back Yoke (BY) of both rotors as well as MPs, and the amplitudes, angular velocities, and the orders of these space harmonics have different characteristics depending on the positions of the CMG. Thus, the effect of space harmonics on the electromagnetic performance of the CMG should be analyzed considering the location of damper bars.

Figure 1 shows the proposed magnetic gear models which are the Surface-mounted Permanent Magnet (SPM) type CMGs with damper bars in the inner rotor BY, outer rotor BY and MPs. Table 1 shows the basic specifications of the analyses models. Each model uses the inner rotor as input, the outer rotor as output, and the MPs as fixed modulator, respectively. As shown in Figure 1, the SPM type CMGs which geometric values are completely same are divided into 4 cases to compare how their dynamic characteristics vary depending on the location of damper bars. In the Case IV having the damper bars in MPs, the damper bars are positioned in the center of all MPs. The reason why other cases have damper bars behind the PM will be described in a following chapter. Although the analysis results may appear differently when the shape, size, and the number of damper bars changes, this paper focuses on the dynamic characteristics according to the position of damper bars for each rotor. In the analyses of this paper use 2D Finite Element Analysis (FEA) method using 2D models of Figure 1. The space harmonic characteristics of magnetic flux density and damping effect of four different models are analyzed through the dynamic analyses and are organized as follows.

(1) Through the analyses of the magnetic flux density distribution at BY & airgap, the amplitudes, angular velocities and orders of the space harmonic components are separated.
(2) The magnitude and frequency of the magnetic flux density with time at the inner & outer BY and MPs under the steady state are analyzed to identify the effect of each space harmonics with time.

(3) The damping effects on the gear performances are compared under different conditions, namely, steady state and transient state including blocked inner rotor.

A detailed step by step descriptions of each analysis are mentioned in the following sections.

II. MAGNETIC FLUX DENSITY CHARACTERISTICS

A. PRINCIPLE OF THE MAGNETIC FIELD MODULATION EFFECT

In CMG, the radial component of modulated magnetic flux density in the airgap is defined by multiplying of the magnetomotive force (MMF) by the permanent magnet (PM) and the permeance function of the MPs as follows [8].

$$\begin{aligned} B_r(r,\theta) &= \sum_m F_{rm}\cos\{mp(\theta-\omega_{PM}t)+mp\theta_0\} \\ &\quad\cdot\left[P_{r0}+\sum_k P_{rk}\cos\{P_{rk}kn_s(\theta-\omega_{MPs}t)\}\right] \\ &= P_{r0}\sum_m F_{rm}\cos\{mp(\theta-\omega_{PM}t)+mp\theta_0\} \\ &\quad+\frac{1}{2}\sum_m\sum_k P_{rk}F_{rm}\cos \\ &\quad\times\left[\cdot\left\{\theta-\left(\frac{mp\omega_{PM}+kn_s\omega_{MPs}}{mp+kn_s}\right)t\right\}\right. \\ &\quad\left.\begin{matrix}(mp+kn_s)\\ +mp\theta_0\end{matrix}\right] \\ &\quad+\frac{1}{2}\sum_m\sum_k P_{rk}F_{rm}\cos \\ &\quad\times\left[\cdot\left\{\theta-\left(\frac{mp\omega_{PM}-kn_s\omega_{MPs}}{mp-kn_s}\right)t\right\}\right. \\ &\quad\left.\begin{matrix}(mp-kn_s)\\ +mp\theta_0\end{matrix}\right] \end{aligned} \tag{1}$$

where, P_{rk} is the k order space harmonic amplitude of permeance distribution, F_{rm} is the m order space harmonic amplitude of MMF, m and k are the space harmonic orders of the MMF and permeance function, p and n_s are the number of rotor pole pair and MPs, ω_{PM} and ω_{MPs} are the angular velocity of rotor and MPs, respectively. As shown in (1), the order and angular velocity of each space harmonic areas follows [8]

$$p_{m,k} = |mp \pm kn_s| \tag{2}$$

$$\omega_{m,k} = \frac{mp}{mp\pm kn_s}\omega_{PM} \pm \frac{kn_s}{mp\pm kn_s}\omega_{MPs} \tag{3}$$

In particular, since the magnitude of the harmonic component modulated with the order of $m = 1, k = -1$ is dominant in the airgap, it is used as a torque producing harmonic, called working harmonic. Among the space harmonics, only the working harmonic produced by on side rotor is in synchronization with the other side rotor and contributes to the useful torque production. The space harmonic orders of the analyses models determined by (2) are summarized in Table 2. Figure 2 is the schematic illustration showing induced

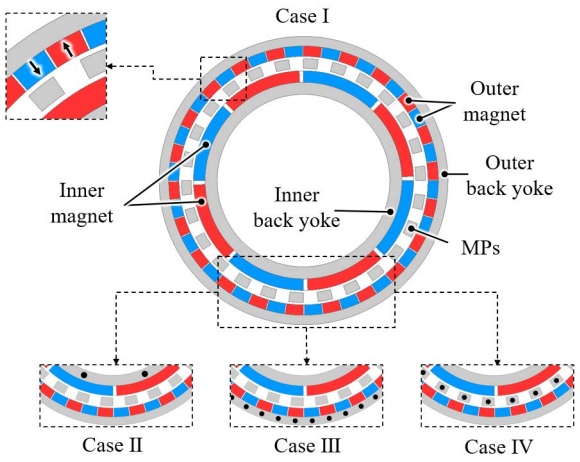

FIGURE 1. Proposed magnetic gear models considering damper bar locations.

TABLE 1. Basic specifications of analyses models.

Parameter	Value
Total diameter (mm)	120
Axial length (mm)	30
Number of pole (In/MPs/Out)	8/26/44
Bar diameter (mm)	2.4
Input speed (RPM)	1500

Classification	Damper bar location	Number of damper bar
Case I	Without damper bar	-
Case II	Inner BY damper bar	8
Case III	Outer BY damper bar	44
Case IV	MPs damper bar	26

current on the damper bar. It is assumed that only the radial components of the magnetic flux density induce current on the damper bar and it can be expressed as (4)

$$\Phi_{ind} = \int_{A_{damper}} \boldsymbol{B_{mod}}\cdot d\boldsymbol{A} \tag{4}$$

where, Φ_{ind}, $\boldsymbol{B_{mod}}$, $d\boldsymbol{A}$ are the magnetic flux that induces the current in the damper bar, modulated magnetic flux density, and a differential surface element enclosed by the damper bars, respectively.

B. SPATIAL MAGNETIC FLUX DENSITY DISTRIBUTION ON BY & AIRGAP

Figure 3 shows the radial flux density characteristics of the inner and outer part of the Case I, where Figure 3(a) and (b) are the flux density distributions in both airgaps and rotor BYs, Figure 3(c) and (d) are their harmonic spectral, respectively. In Figure 3, m_h and m_l are the harmonic orders introduced by the inner and outer rotor PMs, respectively. The magnitude of each space harmonics is significantly decreased when it passes through the airgap and reaches the BY of the opposite side rotor. The main characteristic difference in the space harmonics between the inner and outer rotor BY is the magnitude and the ratio of the unmodulated harmonics to

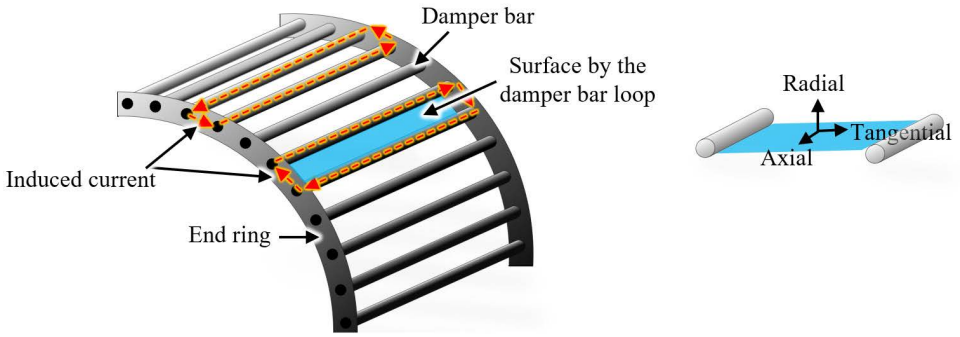

FIGURE 2. Schematic illustration showing induced current on the damper bar.

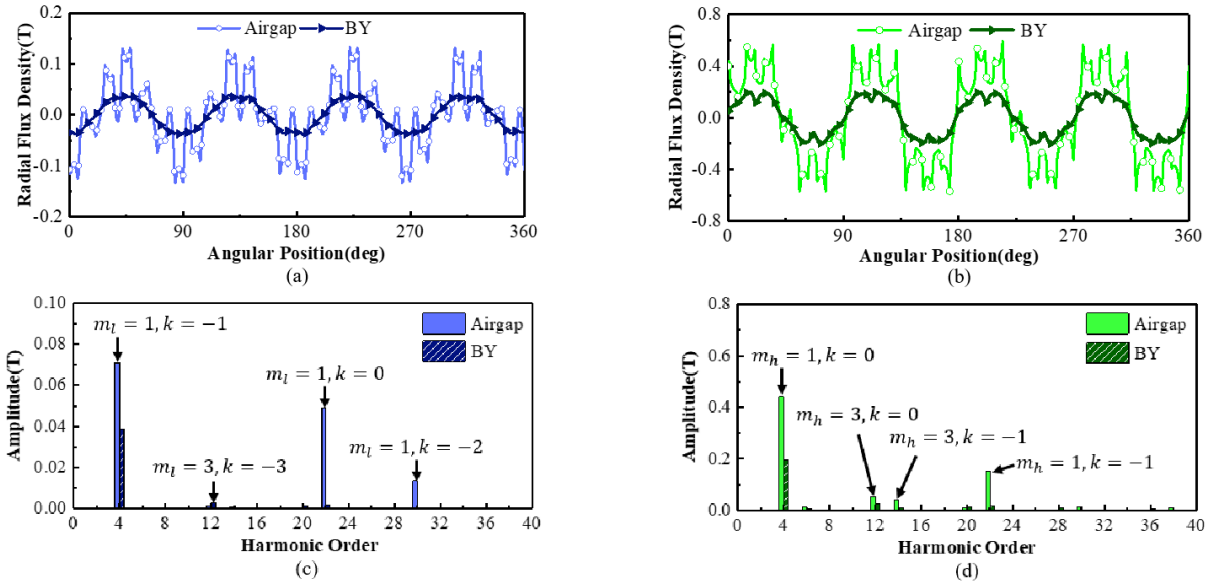

FIGURE 3. Radial flux density characteristics of Case I, (a) flux density distribution at the inner BY and airgap (b) flux density distribution at the outer BY and airgap (c) spectral analysis of flux densities at inner BY and airgap (d) spectral analysis of flux densities at outer BY and airgap.

TABLE 2. Space harmonic orders in the airgap and BY of the analyses models.

k		m_h						m_l					
		1		3		5		1		3		5	
0		4		12		20		22		66		110	
1	-1	30	22	38	14	46	6	48	4	92	40	136	84
2	-2	56	48	64	40	72	32	74	30	118	14	162	58
3	-3	82	74	90	66	98	58	100	56	144	12	188	32

the working harmonic. As shown in Figure 3(c), the working harmonic component, $m_l = 1, k = -1$ is dominant compared to the other space harmonics at inner airgap whereas the unmodulated harmonic component, $m_h = 1, k = 0$ is dominant at the outer airgap, shown in Figure 3(d). This is due to the gear ratio of the CMG model used for the analyses which is 5.5. In the CMG with high gear ratio, the difference in the number of poles between the inner and the outer rotors is large. As a result, the PMs of the inner rotor with a low number of poles influence more significantly to the outer airgap due to abundant magnetic flux and the long flux path. This is the cause of the production of the unmodulated harmonic with higher amplitude than that of the working harmonic at the outer airgap.

C. TEMPORAL FLUX DENSITY DISTRIBUTION ON BY & MPs

Figure 4 shows the analyses points to measure the variation of the magnitude and frequency of the magnetic flux density with time at the inner BY, outer BY and MPs in Case I. Figure 5(a), (b) and (c) are the variations of the magnetic flux density in the steady state based on the analyses points

in Figure 4. The point 1 and 2 are the locations on BY behind the center of PM and the pole transition region, respectively. The variation frequencies for the magnetic flux densities in Figure 5 are determined by the relative speed between the rotor and the magnetic flux density harmonics as follows

$$\omega_{relative} = \left|\boldsymbol{\omega_{m,k}} - \boldsymbol{\omega_{rot}}\right| \tag{5}$$

where, $\boldsymbol{\omega_{rot}}$ is the angular velocity of the rotor for the calculation of $\omega_{relative}$. Then, the variation frequency of the radial magnetic flux density is expressed as follows

$$f_{Br} = \left\{\frac{\omega_{relative} \cdot p_{m,k}}{2\pi}\right\} \tag{6}$$

To investigate on how the variation of the space harmonics affects the BY during the operation of the CMG, the magnetic flux density variation with time on the outer BY is considered. The variations of the magnetic flux density on the outer BY is caused by the inner rotor PM. Accordingly, ω_{PM} in (3) is 1500 RPM, which is the rotational speed of the inner rotor in the steady state. Also, ω_{MPs} equals to zero because the MPs in the analysis models are stationary. Now using (3) and (5), following analyses results can be reached

1) The rotational speed of the unmodulated harmonic with highest amplitude is determined as

$$\omega_{1,0} = \omega_{PM} = \omega_{in} \tag{7}$$

where, ω_{in} is the rotational speed of the inner rotor. Then, $\omega_{relative}$ is calculated with the rotational speed of the outer rotor, ω_{out} as follows

$$\omega_{relative\_1} = \left|\boldsymbol{\omega_{1,0}} - \boldsymbol{\omega_{out}}\right| = \omega_{in} + \omega_{out} \tag{8}$$

When the MPs are stationary, the inner and the outer rotors rotate in counterrotating manner. Therefore, the relative speed between the unmodulated harmonic and the outer rotor, $\omega_{relative\_1}$ is always the sum of the speeds of the two rotors. For this reason, when input side of the CMG is rotated, the relative speed of the unmodulated harmonic is bigger than the input speed all the time and as the input speed is getting faster, the influence of the unmodulated harmonic on the electromagnetic performance of the CMG with damper bar at the outer BY becomes greater.

2) The rotational speed of the modulated harmonic with highest amplitude, working harmonic in the steady state is determined as

$$\omega_{1,-1} = \omega_{out} \tag{9}$$

Thus, using (5) and (9), the relative speed between the working harmonic and the outer rotor, $\omega_{relative\_2}$ is zero in the steady state as follows

$$\omega_{relative\_2} = \left|\boldsymbol{\omega_{1,-1}} - \boldsymbol{\omega_{out}}\right| = \omega_{out} - \omega_{out} = 0 \tag{10}$$

Unlike the unmodulated harmonics, the relative speed caused by working harmonic only arises when the steady state is interrupted by mechanical loading or speed changes

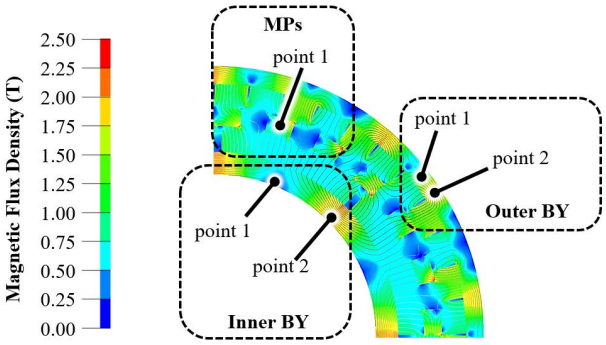

FIGURE 4. Analysis point to measure magnetic flux density with time.

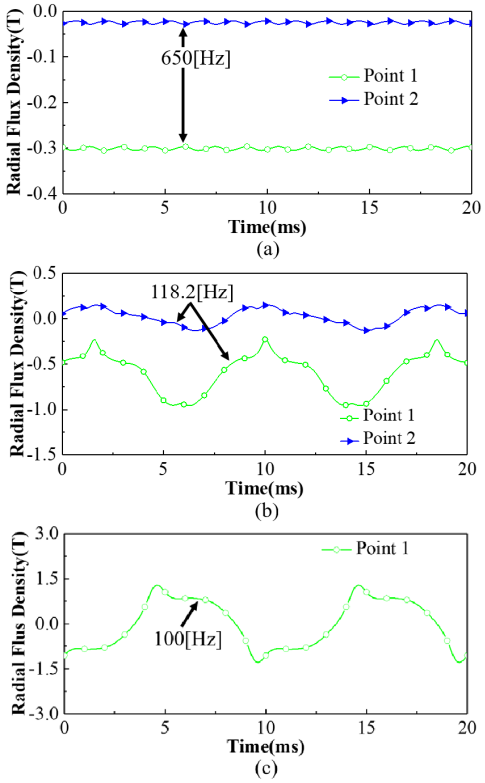

FIGURE 5. Variation of the radial magnetic flux density over half mechanical period of the inner rotor in the steady state operation (a) inner BY (b) outer BY (c) MPs.

Therefore, the variation of the magnetic flux density in Figure 5(a) and Figure 5(b) are only caused by the asynchronous harmonics including the unmodulated harmonics. Also, by checking the harmonic frequency using (6), it is clear that the most influential harmonic among the asynchronous harmonics at the outer BY is the unmodulated harmonic, $m_h = 1, k = 0$ in the steady state, and it is calculated as 118.2 Hz as shown in Figure 5(b). When the above process is applied to the inner BY, the most influential harmonic is $m_l = 1, k = 0$ in the steady state, and it is calculated as 650 Hz as shown in Figure 5(a).

Meanwhile, the relative speed between the MPs and the magnetic flux density harmonics is calculated differently. The magnetic fluxes coming from the one side PMs reach the other side airgap after passing through the fixed MPs. Unlike the inner and outer rotor BYs, only the unmodulated harmonic component exist inside the MPs. Accordingly, from (2) and (3), the order and speed of each space harmonic in MPs are expressed as follows

$$p_{m,k} = mp \tag{11}$$

$$\omega_{m,k} = \omega_{rot} \tag{12}$$

Considering (5) and (12), $\omega_{relative}$ between the harmonics by the inner rotor PM and the MPs is equal to the ω_{in}. Similarly, $\omega_{relative}$ between the harmonics by the outer rotor PM and the MPs is equal to the ω_{out}. Considering (6) and (11), the product of ω_{in} and m_h is same as the product of ω_{out} and m_l. In the steady state, the unmodulated harmonics of each rotor, which have the same order of m, form the same variation frequency in the MPs. As shown in Figure 5(c), the dominant frequency in MPs is identified as 100 Hz, and formed by the $m = 1$ harmonics of each rotor PMs. As shown in Figure 5(a), (b) and (c), the magnitudes of the magnetic flux density variation with time is the largest in the MPs and the smallest in the inner BY. For this reason, the damper bar current in Case IV of Figure 1 can be higher than those in other damper bar models. Consequently, the torque reduction is also expected to be higher for Case IV.

Meanwhile, the magnetic saturation influences the variation of the magnetic flux density at the BY with time. As shown in Figure 5(a) and (b), the magnetic flux density at point 1 corresponding to the position behind the center of PM, has higher fluctuation than point 2, the pole transition region. Based on this observation, the damper bar position of BY is selected behind the center of PM. Therefore, The damper bars of MPs are located in all MPs, and one damper bar is located in the center of each MPs.

III. DYNAMIC MODELING OF OUTER ROTOR

The outer rotor should be dynamically modeled to determine how the damper bar influences the mechanical output. The dynamic equation of motion of the outer rotor is shown below

$$T - T_L = J\frac{d^2\theta}{dt^2} + B\frac{d\theta}{dt} + K\theta \tag{13}$$

where T, T_L, J, B, K, θ is the outer rotor torque, the load torque, the moment of inertia of outer rotor, the viscous friction coefficient, the torsional spring coefficient and the mechanical angle, respectively. The dynamic modeling procedure is composed of following steps

1) J is calculated using the dimension and the mass of the
2) outer rotor as shown in Table 3.
3) The hunting action of outer rotor is equivalized as spring movement. Thus, K of outer rotor is calculated by measuring the pull-out torque in electrical half period as shown in Figure 6 [30]–[32].

$$K = \frac{T_{pullout}}{\theta_k} \tag{14}$$

where $T_{pullout}$ and θ_k are the pull-out torque and mechanical angle of electrical half period of outer rotor, respectively.

4) As for the friction element of magnetic gear, only the bearing friction with light damping is considered having damping ratio ξ given as

$$\xi = \frac{B}{2\sqrt{JK}} \tag{15}$$

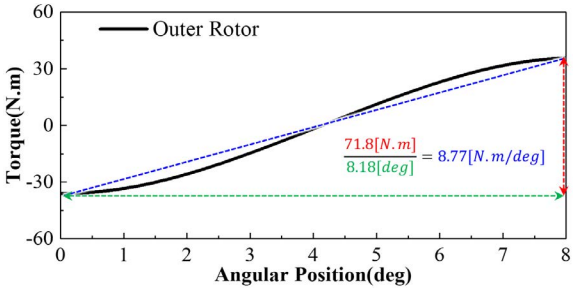

FIGURE 6. Stiffness coefficient calculation method by linearizing of the pull-out torque.

TABLE 3. Specifications for the moment of inertia of the outer rotor.

Sector	Core	Magnet
Material	35PN440	NdFeB
Specific gravity	7.7	7.4
Mass (kg)	0.33	0.31
Moment of inertia (kg·m^2)	0.0012	0.0008

IV. DAMPER BAR EFFECT ANALYSIS

A. STEADY STATE ANALYSIS

Figure 7 shows the steady state analysis of the Case I which is the model without damper bar with Figure 7(a) showing the inner and outer rotor torque and Figure 7(b) showing the inner and outer rotor angular velocity, respectively. From Figure 7, the two rotors are kept at the full load angle and rotated at a set speed, 1500 rpm for the inner rotor and 272.72 rpm for the outer rotor. The full load torque of Case I for the inner and outer rotors are 6.5 N.m and 35.9 N.m, respectively. Figure 8(a) and (b) show the outer rotor torque and the induced current in one bar for the three models with damper b ars, respectively. For Case II, III, and IV in Figure 8, the analysis conditions are same with the steady state analysis of Case I. The full load average torque and damper bar current values are summarized in Table 4. For the comparison of the analyses results, the amplitudes of current of damper bars represents to the root mean square values of dominant harmonic.

In the steady state, as already shown in Figure 5, the source of variation of the magnetic flux density in each BY is not the working harmonic, but the asynchronous harmonics

including the unmodulated harmonics. Thus, the dominant harmonic component inducing the current on the damper bars is the unmodulated harmonic, having $m_h = 1, k = 0$. In Case II, the variation of the magnetic flux density with time is small as shown in Figure 5(a), and thus the induced current is negligible as $0.03A_{rms}$, shown in Figure 8(b) and Table 4. Therefore, the torque of Case II is almost same with Case I. In Case III and Case IV, however, the induced currents in the damper bar are $294.8A_{rms}$ and $687.4A_{rms}$. These induced currents act as losses in the steady state and result in the reduction of the output torque. Compared to the full load average torque of Case I, Case III is decreased by 6.4% and Case IV decreased by 14.2%. As the induced current in the damper bar increases, the transmitted torque decreases.

For the CMG models with high gear ratio, such as in this paper, the difference of the magnetic flux density characteristics between the inner and outer rotor BYs is even greater. The inner rotor BY has a relatively smaller amplitude of space harmonics compared to the outer rotor BY. Besides, the dominant harmonic component of the magnetic flux density of inner rotor BY is the working harmonic. However, the outer rotor BY has a relatively higher amplitude of space harmonics and the unmodulated harmonic among the asynchronous harmonics is dominant. Therefore, in the steady state, the amplitude of induced current in Case III, which has the outer rotor damper bar is much larger than that in Case II, where the damper bars are placed on the inner rotor. On the other hand, the stationary MPs are not synchronized with any magnetic flux density harmonic component and the amplitude of the variation of magnetic flux density with time is the largest compared to the inner and the outer rotor BYs. Thus, in the steady state, the amplitude of the induced current in Case IV, which has damper bars on MPs, is the largest.

B. TRANSIENT STATE ANALYSIS WITH BLOCKED INNER ROTOR

Figure 9 shows the settling time analysis of Case I when the inner rotor is blocked. Figure 9(a) shows the torques of the inner and outer rotors and Figure 9(b) represents the angular positions of inner and outer rotors. The analysis is composed of following steps

(A) Fixing the inner and outer rotors to full load angle
(B) Releasing the outer rotor only

Following steps (A) and (B), the outer rotor produces spring movement by generating torque as shown in Figure 9(b). Since there is no external input, the torques in both rotors are converged to zero and the outer rotor is positioned to the noload angle. The settling time is defined as the time required for the torque curve to reach and stay within a range of 2% of the final torque [35]. Figure 10 shows the settling time analysis of Case II, III, and IV with the same analysis condition of Case I. Figure 10(a) and (b) show the torque and angular position of the outer rotor. Similarly, Figure 10(c) and (d) show the torque and angular position of the inner rotor, respectively.

As confirmed from the CMG's magnetic flux density characteristics, once the CMG rotates, the asynchronous harmonics varies with time in the BY irrespective of the changes in load angle. In particular, the most dominant component among the asynchronous harmonics is the unmodulated harmonic. In this case, considering (5), the relative speed between this harmonic and outer rotor, $\omega_{relative\_1}$ is same as the speed of the outer rotor due to the stationary inner rotor. Therefore, it is clear that the effect of asynchronous harmonics is the smallest at this analysis situation. Once the inner rotor starts to rotate, ω_{in} increases, and the $\omega_{relative\_1}$ is getting increased.

However, the relative speed of the working harmonic and the outer rotor, $\omega_{relative\_2}$ is not affected by the input speed. The asynchronization between the working harmonics and the outer rotor exists only during the changes in load angle. For this reason, the transient state analysis with blocked inner rotor is the best way to minimize the effect of asynchronous harmonics while holding on the effect of the working harmonic. The settling time by the damping effect in each case is compared with Table 5. Considering the Figure 10 and Table 5, each case can be analyzed as follows

1) Case II: As shown in Table 5, the damping effect is negligible and the settling time is not changed compared to Case I. This signifies the working harmonic effect to the damper bar in Case II is too small to affect the settling time. Considering the results of the steady state analysis from Figure 8 and Table 4, it can be expected that the asynchronous harmonics in Case II also have negligible effect on damper bars even under the application of the input speed.
2) Case III: As shown in Table 5, although the damping force affects the settling time, it only reduces by 0.8% compared to Case I. This means the working harmonic induces the small current on the damper bar. However, considering the steady state analysis from Figure 8, the damping effect can be increased by the asynchronous harmonics when the input speed is applied.
3) Case IV: The reduction rate of settling time due to the damping effect is 11.8%, which is the largest among the three cases. In MPs, all magnetic flux density harmonics stay unmodulated and have significant magnitude than those of the inner and outer rotor BY. Therefore, the variation of the magnetic flux density with time is the highest compared the other two cases. As a result, the settling time improvement is the best.

C. TRANSIENT STATE ANALYSIS WITH LOAD CHANGES

Figure 11 shows the settling time analysis of Case I with load changes. Figure 11(a) and (b) show the torque and the rotational speed of the inner and the outer rotors. The analysis is composed of following steps

(A) Applying a load of 5 N.m to the outer rotor of the CMG operating on the steady state

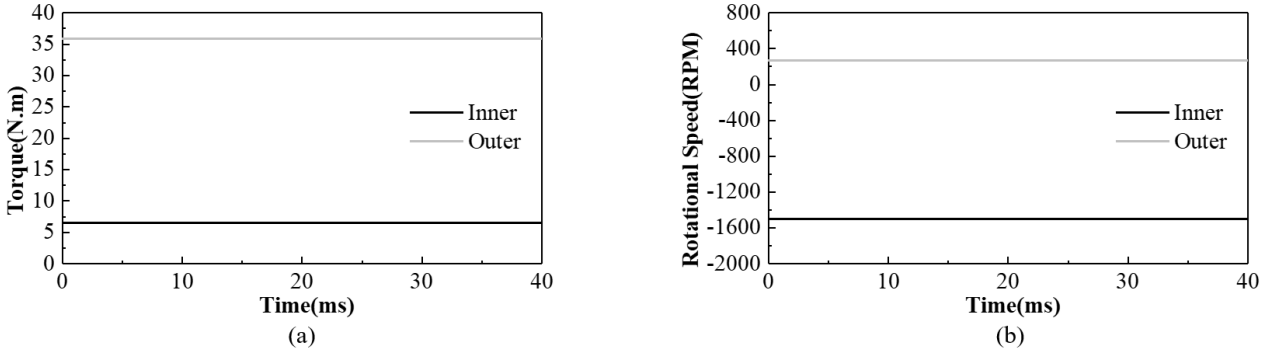

FIGURE 7. Steady state analysis of Case I (a) torque of inner and outer rotor (b) rotational speed of inner and outer rotor.

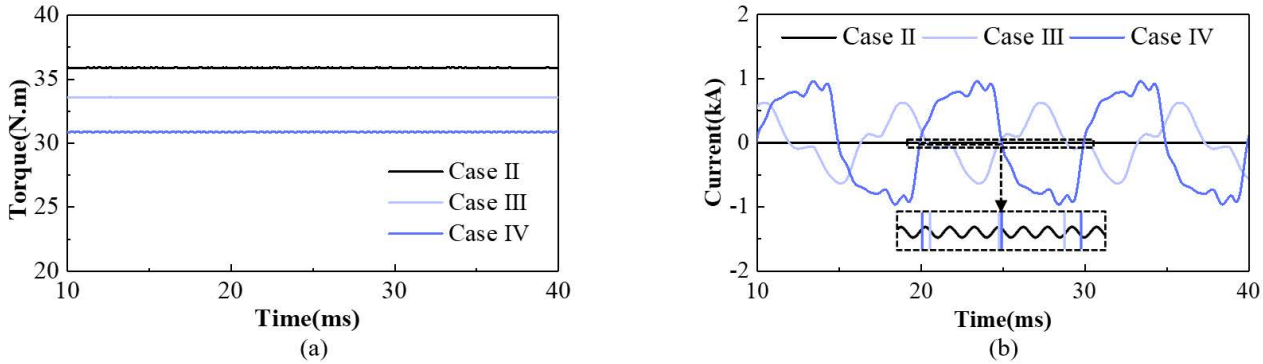

FIGURE 8. Steady state analysis of Case II, Case III, and Case IV, (a) torque of outer rotor, (b) induced current of one bar.

TABLE 4. Specifications for the moment of inertia of the outer rotor.

Model	Full load average torque (N·m)	Dominant harmonic amplitude of damper bar current (A_{rms})
Case I	35.9 (100%)	-
Case II	35.9 (100%)	0.03
Case III	33.6 (93.6%)	294.8
Case IV	30.8 (85.8%)	687.4

(B) Maintaining the load until the speed of outer rotor is stabilized

(C) Applying an additional load of 10 N.m to the outer rotor and keeping the state until the speed of outer rotor stabilizes.

Following steps (A) - (C), the outer rotor produces hunting around the steady state speed while the inner rotor is kept at the constant speed of 1500 RPM. as shown in Figure 11(b). In this analysis, the equation of motion includes the friction torque of ball bearings according to the rotor speed. Figure 12 shows the settling time analysis of Case II, III, and IV. Figure 12(a) and (b) show the torque and rotational speed of the outer rotor. Similarly, Figure 12(c) and (d) show the torque and rotational speed of the inner rotor, respectively. Also, the analysis conditions are same with the settling time analysis of Case I in Figure 11. The damping effect of dynamic state in each case are summarized in Table 6.

Considering (5), It is obvious that the relative speed between the unmodulated harmonic and the outer rotor, $\omega_{relative\_1}$ can be increased with the rotational speed of the inner rotor. For this reason, through this analysis, it is possible to confirm the damping effect caused by the asynchronous harmonics due to the increase of the inner rotor speed. Also, the important consideration of this analysis is that the damping effect by the working harmonic occurs only when the load angle fluctuates, and it is same as the transient state analyses with blocked inner rotor. Therefore, the difference in the reduction rate of the settling time in Table 5 and Table 6 is caused by the effect of the asynchronous harmonics with increased rotational speed of the inner rotor. Considering the Figure 12 and Table 6, each case can be analyzed as follows

1) Case II: As shown in Table 6, the settling time is not reduced compared to the Case I. The unmodulated harmonics does not create enough damping effect to influence the settling time.
2) Case III: As shown in Table 6, the settling time is reduced by 3.2% compared to the Case I. With the comparison to the results in Table 5, the reduction rate of the settling time increases from 0.8% to 3.2%. The

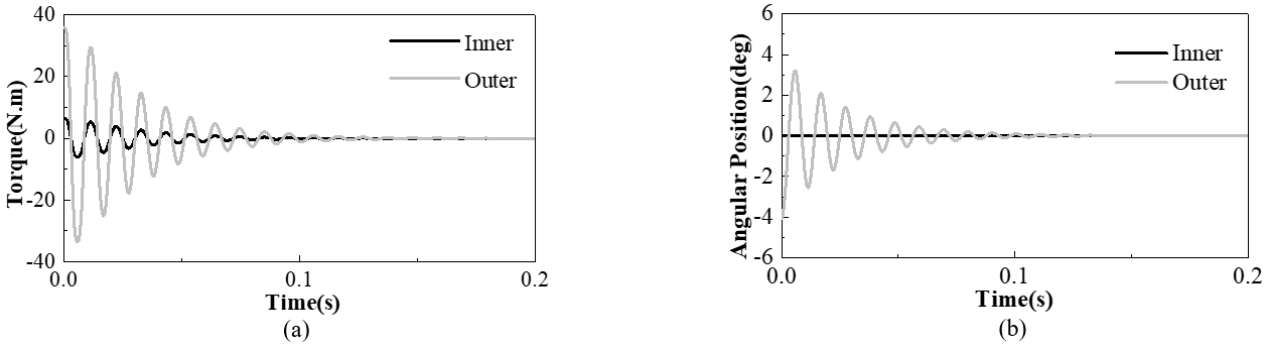

FIGURE 9. Settling time analysis of Case I when the inner rotor is blocked: (a) torque of inner and outer rotor (b) angular position of inner and outer rotor.

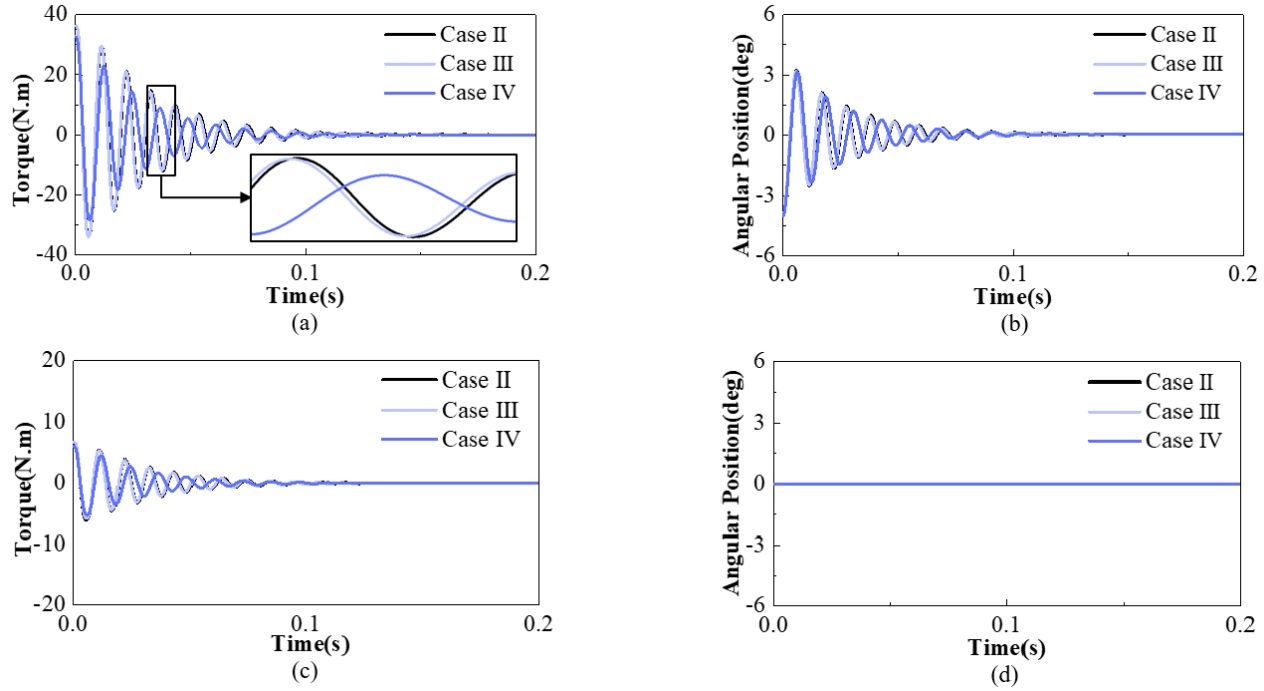

FIGURE 10. Settling time analysis of Case II, Case III, and Case IV when the inner rotor is blocked: (a) torque of outer rotor (b) angular position of outer rotor (c) torque of inner rotor (d) angular position of inner rotor.

TABLE 5. Analyses results of settling time with blocked inner rotor.

Model	Settling time (ms)	Decrease rate of settling time (%)
Case I	137	-
Case II	137	0
Case III	136	0.8
Case IV	121	11.7

increase in this reduction rate is due to the increase in the damping effect of the unmodulated harmonic. However, the required torque in the inner rotor to produce the same load torque is also increased by 2.1 times compared to the Case I. It is clear disadvantage that the ratio of torque reduction is greater than the settling time reduction.

3) Case IV: The reduction rate of the settling time is 12.8%, the largest reduction among the three cases. However, the required torque of the inner rotor is also increased by 3.5 times. Due to the magnetic flux density characteristics of stationary MPs, Case IV has the highest torque reduction by the induced current of the damper bar.

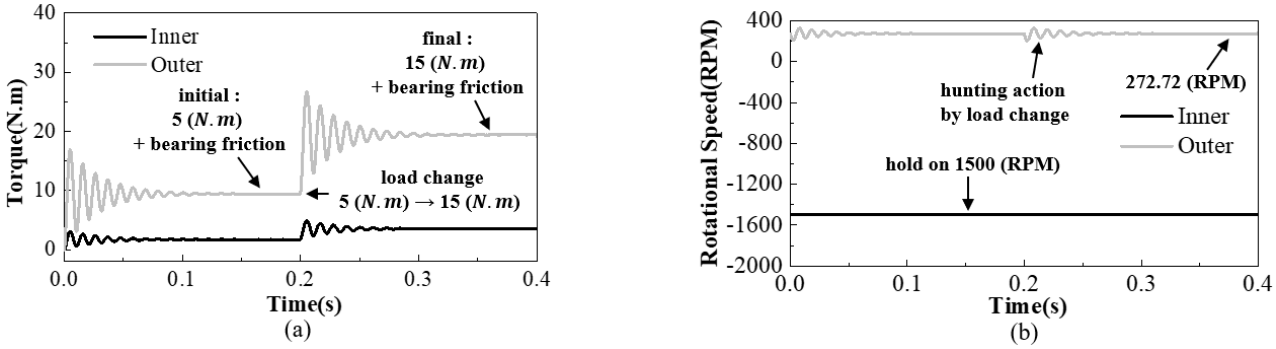

FIGURE 11. Settling time analysis of Case I with load changes: (a) torque of inner and outer rotor (b) rotational speed of inner and outer rotor.

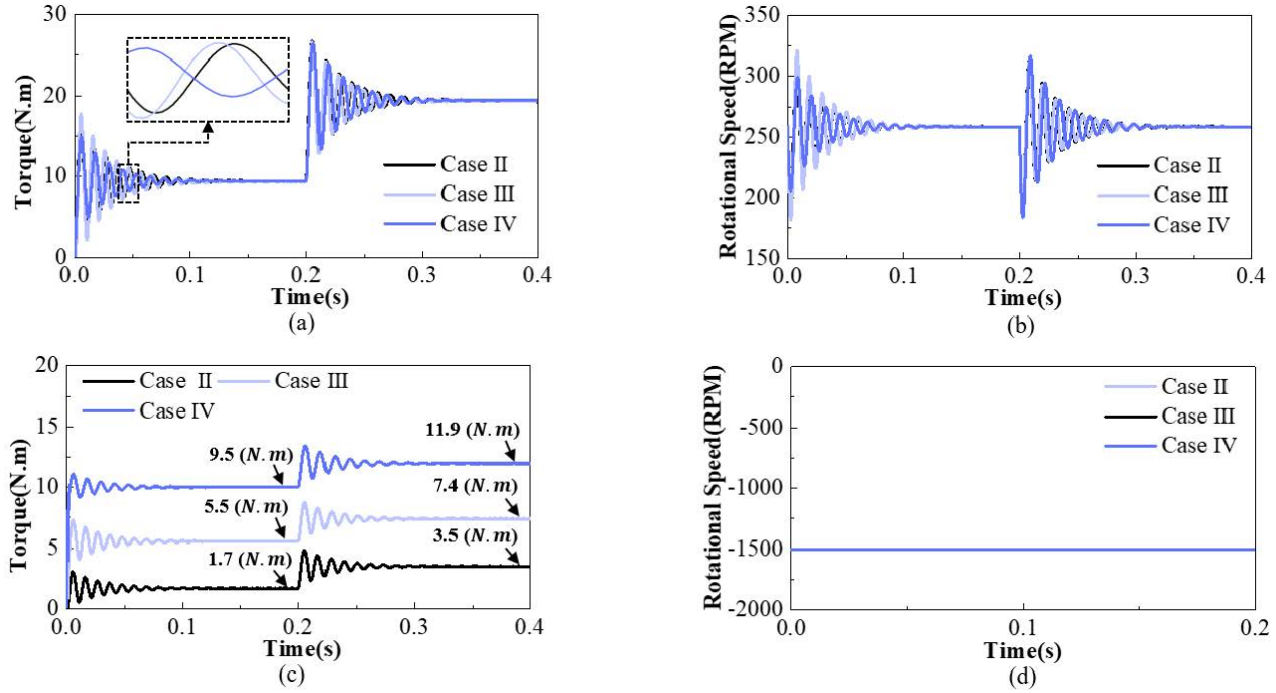

FIGURE 12. Settling time analysis of Case II, Case III, and Case IV with load changes: (a) torque of outer rotor (b) rotational speed of outer rotor (c) torque of inner rotor (d) rotational speed of inner rotor.

TABLE 6. Analyses results of settling time with load changes.

Model	Settling time (ms)	Input torque at 0.4s (N.m)
Case I	125 (100%)	3.5 (100%)
Case II	125 (100%)	3.5 (100%)
Case III	121 (96.8%)	7.4 (210%)
Case IV	109 (87.2%)	11.9 (350%)

From the analyses results, the inner BY damper bar model does not show significant effect on the torque reduction and settling time improvement. The MPs damper bar model, however, shows the largest settling time and torque reductions among the three analyses models. Finally, the outer BY damper bar model also shows both torque and settling time reductions which are in between the MPs and the inner BY damper bar models. Therefore, considering the damping effect of the magnetic gear, the superior characteristics are in the order of the MPs damper bar model followed by the outer rotor BY and inner rotor BY damper bar models, respectively. However, the transmitted torque reduction caused by the

induced current on the damper bars should also be considered during the operation of the magnetic gear. The torque reduction increases as the damping effect improves.

V. CONCLUSION

In conclusion, by the comprehensive analysis of the influence of damper bars on CMG characteristics, the space harmonics of the magnetic flux density, settling time of the output rotor and reduction of the transmitted torque by the damping effect are characterized and the results can be summarized as follows

1) The asynchronous harmonics not only reduce the steady state torque but also affect damping effect during the transient states of outer rotor. As the rotor speed increases, the torque reduction and the damping force increase simultaneously. However, the working harmonic does not induce the current in the damper bar in the steady state of the rotor. It can induces the current in the damper bar when the load angle is only changed.
2) The damping effect of SPM type CMG is analyzed for three different cases depending on the positions of the damper bars. In the case of the inner rotor BY, the variation of magnetic flux density with time is small, and both the torque reduction and the damping effect are negligible. The outer rotor BY damper bar model shows both torque and settling time reductions which are in between the inner rotor BY and MPs damper bar models. It should be considered in the outer rotor BY damper bar model that the ratio of transmitted torque reduction is greater than the settling time reduction. The MPs damper bar model has the largest effects in both of the settling time and torque reduction among three analyses models. When considering the settling time only, MPs damper bar model is the best, but the torque reduction is also the highest.
3) The torque reduction caused by asynchronous harmonics is proportional to the rotational speed. Therefore, the damper bars should be used cautiously during the high speed applications of the CMG.

REFERENCES

[1] J. Zhou, W. Sun, and L. Cao, "Vibration and noise characteristics of a gear reducer under different operation conditions," *J. Low Freq. Noise, Vib. Act. Control*, vol. 38, no. 2, pp. 574–591, Jun. 2019.

[2] M. S. Abbes, S. Bouaziz, F. Chaari, M. Maatar, and M. Haddar, "An acoustic–structural interaction modelling for the evaluation of a gearbox-radiated noise," *Int. J. Mech. Sci.*, vol. 50, no. 3, pp. 569–577, Mar. 2008.

[3] M. Barthod, B. Hayne, J.-L. Tébec, and J.-C. Pin, "Experimental study of dynamic and noise produced by a gearing excited by a multi-harmonic excitation," *Appl. Acoust.*, vol. 68, no. 9, pp. 982–1002, Sep. 2007.

[4] G. Liu and R. G. Parker, "Nonlinear, parametrically excited dynamics of two-stage spur gear trains with mesh stiffness fluctuation," *Proc. Inst. Mech. Eng., C, J. Mech. Eng. Sci.*, vol. 226, no. 8, pp. 1939–1957, Aug. 2012.

[5] J. Lin and R. G. Parker, "Mesh stiffness variation instabilities in two-stage gear systems," *J. Vib. Acoust.*, vol. 124, no. 1, pp. 68–76, Sep. 2001.

[6] K. Tsurumoto and S. Kikuchi, "A new magnetic gear using permanent magnet," *IEEE Trans. Magn.*, vol. 23, no. 5, pp. 3622–3624, Sep. 1987.

[7] K. Tsurumoto, "Generating mechanism of magnetic force in meshing area of magnetic gear using permanent magnet," *IEEE Transl. J. Magn. Jpn.*, vol. 6, no. 6, pp. 531–536, Jun. 1991.

[8] K. Atallah and D. Howe, "A novel high-performance magnetic gear," *IEEE Trans. Magn.*, vol. 37, no. 4, pp. 2844–2846, Jul. 2001.

[9] Z. Tang, P. Liu, Y. Chen, and H. Guo, "Experimental study of counter-rotating propellers for high-altitude airships," *J. Propuls. Power*, vol. 31, no. 5, pp. 1491–1496, Sep. 2015.

[10] X. Wei, B. Huang, P. Liu, T. Kanemoto, and L. Wang, "Experimental investigation into the effects of blade pitch angle and axial distance on the performance of a counter-rotating tidal turbine," *Ocean Eng.*, vol. 110, pp. 78–88, Dec. 2015.

[11] V. A. Koehuan and S. Kamal, "Investigation of counter-rotating wind turbine performance using computational fluid dynamics simulation," in *Proc. IOP Conf., Mater. Sci. Eng.*, 2017, Art. no. 012034, doi: 10.1088/1757-899X/267/1/012034.

[12] Z. Tang, P. Liu, J. Sun, Y. Chen, H. Guo, and G. Li, "Performance of contra-rotating propellers for stratospheric airships," *Int. J. Aeronaut. Space Sci.*, vol. 16, no. 4, pp. 485–492, Dec. 2015.

[13] H. Shin, J. Chang, and D. Hong, "Design and characteristics analysis of coaxial magnetic gear for contra-rotating propeller in yacht," *IEEE Trans. Ind. Electron.*, vol. 67, no. 9, pp. 7250–7259, Sep. 2020.

[14] M. C. Gardner, M. Johnson, and H. A. Toliyat, "Analysis of high gear ratio capabilities for single-stage, series multistage, and compound differential coaxial magnetic gears," *IEEE Trans. Energy Convers.*, vol. 34, no. 2, pp. 665–672, Jun. 2019.

[15] E. Gobl, G. Jungmayr, E. Marth, and W. Amrhein, "Optimization and comparison of coaxial magnetic gears with and without back iron," *IEEE Trans. Magn.*, vol. 54, no. 11, pp. 1–4, Nov. 2018.

[16] J. Lee and J. Chang, "Analysis of the vibration characteristics of coaxial magnetic gear," *IEEE Trans. Magn.*, vol. 53, no. 6, pp. 1–4, Jun. 2017.

[17] H. Y. Wong, J. Z. Bird, S. Modaresahmadi, and W. Williams, "Comparative analysis of a coaxial magnetic gear with a flux concentration rotor and consequent pole rotor typology," *IEEE Trans. Magn.*, vol. 54, no. 11, pp. 1–5, Nov. 2018.

[18] S. J. Kim, E.-J. Park, S.-Y. Jung, and Y.-J. Kim, "Transfer torque performance comparison in coaxial magnetic gears with different flux-modulator shapes," *IEEE Trans. Magn.*, vol. 53, no. 6, pp. 1–4, Jun. 2017.

[19] J. T. Park, T. W. Lee, D. K. Hong, and J. H. Chang, "Magnetic–mechanical performance analysis and experimental validation of noncontact coaxial magnetic gear for a contra-rotating propeller in an electric outboard," *IEEE Trans. Magn.*, vol. 57, no. 2, Feb. 2021, Art. no. 8202605.

[20] B. Mcgilton, R. Crozier, A. McDonald, and M. Mueller, "Review of magnetic gear technologies and their applications in marine energy," *IET Renew. Power Gener.*, vol. 12, no. 2, pp. 174–181, Dec. 2017.

[21] X. Liu, K. T. Chau, M. Cheng, and W. Hua, "Comparison of magnetic-geard permanent-magnet machines," *Prog. Electromagn. Res.*, vol. 133, pp. 177–198, 2013.

[22] P. O. Rasmussen, T. O. Andersen, F. T. Jorgensen, and O. Nielsen, "Development of a high-performance magnetic gear," *IEEE Trans. Ind. Appl.*, vol. 41, no. 3, pp. 764–770, May 2005.

[23] V. Mateev, M. Todorova, and I. Marinova, "Analysis of flux density harmonic spectrum of the coaxial magnetic gear," in *Proc. 16th Conf. Electr. Mach., Drives Power Syst. (ELMA)*, Jun. 2019, pp. 1–6, doi: 10.1109/ELMA.2019.8771653.

[24] J. Matsuki, T. Katagi, and T. Okada, "Damper windings phenomena of synchronous machines during system oscillations," *IEEE Trans. Energy Convers.*, vol. 9, no. 2, pp. 376–382, Jun. 1994.

[25] M. Ranlöf, J. Bladh, and U. Lundin, "Use of a finite element model for the determination of damping and synchronizing torques of hydroelectric generators," *Int. J. Electr. Power Energy Syst.*, vol. 44, no. 1, pp. 844–851, Jan. 2013.

[26] A. M. A. Oteafy, J. N. Chiasson, and S. Ahmed-Zaid, "Development and application of a standstill parameter identification technique for the synchronous generator," *Int. J. Electr. Power Energy Syst.*, vol. 81, pp. 222–231, Oct. 2016.

[27] X. Lu, K. L. V. Lyer, K. Mukherjee, K. Ramkumar, and N. C. Kar, "Investigation of permanent-magnet motor drives incorporating damper bars for electrified vehicles," *IEEE Trans. Ind. Electron.*, vol. 62, no. 5, pp. 3234–3244, May 2015.

[28] X. Lu, "Dual benefits of adding damper bars in PMSMs for electrified vehicles: Improved machine dynamics and simplified integrated charging," Ph.D. dissertation, Dept. Elect. Comput. Eng., Windsor Univ., Windsor, ON, Canada, Dec. 2014. [Online]. Available: https://scholar.uwindsor.ca/etd/5194/

[29] X. Liu, Y. Zhao, X. Zhang, J. Gao, and S. Huang, "Investigation of the dynamic characteristics of a coaxial magnetic gear under loading condition based on analytical model," in *Proc. 20th Int. Conf. Elect. Mach. Syst. (ICEMS)*, Aug. 2017, pp. 1–5, doi: 10.1109/ICEMS.2017.8055986.
[30] R. Montague, C. Bingham, and K. Atallah, "Servo control of magnetic gears," *IEEE/ASME Trans. Mechatronics*, vol. 17, no. 2, pp. 269–278, Apr. 2012.
[31] C.-L. Chen and M.-C. Tsai, "Kinematic and dynamic analysis of magnetic gear with dual-mechanical port using block diagrams," *IEEE Trans. Magn.*, vol. 54, no. 11, pp. 1–5, Nov. 2018.
[32] W. Nicolas Frank, S. Pakdelian, and A. Hamid Toliyat, "Passive suppression of transient oscillations in the concentric planetary magnetic gear," *IEEE Trans. Energy Convers.*, vol. 26, no. 3, pp. 933–939, Sep. 2011.
[33] B. H. Ma, C. C. Hou, and G. Q. Bao, "Transient behavior of field modulated magnetic gears with damper windings," in *Proc. IEEE Vehicle Power Propuls. Conf. (VPPC)*, Oct. 2016, doi: 10.1109/VPPC.2016.7791808.
[34] Y. Akcay, T. Cox, and A. Costabeber, "Improving magnetic gear overload torque with cage rotor bars," in *Proc. 20th Int. Conf. Electr. Mach. Syst. (ICEMS)*, Aug. 2017, pp. 1–5, doi: 10.1109/ICEMS.2017.8056295.
[35] T. T. Tay, I. M. Y. Mareels, and J. B. Moore, *High Performance Control*. Basel, Switzerland: Birkhäuser, 1998.

SEOKHOON JO (Student Member, IEEE) was born in Anyang, South Korea. He received the B.Sc. and M.Sc. degrees in electrical engineering from Dong-A University, Busan, South Korea, in 2020 and 2022, respectively. His research interests include motor design and drive, such as synchronous motor and magnetic geared motor and design of electro-mechanical systems, such as magnetic gear. He is a Student Member of the Institute of Electrical Engineers, Republic of Korea (KIEE).

HOMIN SHIN (Member, IEEE) was born in Busan, South Korea. He received the B.Sc. and M.Sc. degrees in electrical engineering from Dong-A University, Busan, South Korea, in 2014 and 2016, respectively, where he is currently pursuing the Ph.D. degree in electrical machine design and control. His research interests include motor design and drive, such as synchronous motor, induction motor and magnetic geared motor, and design of electro-mechanical systems, such as electrically driven machine tools and magnetic gear. He is a Student Member of the Institute of Electrical Engineers, Republic of Korea (KIEE).

JUNGHWAN CHANG (Member, IEEE) received the B.S. and M.S. degrees in electrical engineering and the Ph.D. degree in precision mechanical engineering from Hanyang University, Seoul, South Korea, in 1994, 1997, and 2001, respectively. From 2001 to 2002, he was with the Institute of Brain Korea 21, Hanyang University, where he developed micro drive and high-speed spindle motor. From 2002 to 2003, he was a Research Fellow with the University of California at Berkeley, Berkeley, CA, USA, where he analyzed and developed electrically controlled engine valve system. From 2003 to 2009, he was a Technical Leader with the Korea Electrotechnology Research Institute, South Korea, where he was involved in the developments of special purpose machines. Since 2009, he has been a Professor with the Department of Electrical Engineering, Dong-A University, Busan, South Korea. His current research interests include the design and analysis of electromechanical systems, such as electrically driven machine tools and magnetic gear. He is a member of The Korea Institute of Electrical Engineers, South Korea. He was a Steering Committee Member and the Technical Program Chair in different conferences, such as International Conference on Electrical Machines and Systems (ICEMS) 2013, IEEE International Transportation Electrification Conference Asia-Pacific 2016, COMPUMAG 2017, and ICEMS 2018. He is a Reviewer of the IEEE TRANSACTIONS ON MAGNETICS, IEEE TRANSACTIONS ON INDUSTRIAL ELECTRONICS, IEEE TRANSACTIONS ON INDUSTRIAL APPLICATION, and IEEE/ASME TRANSACTIONS ON MECHATRONICS.